KAUNAS UNIVERSITY OF TECHNOLOGY
VYTAUTAS MAGNUS UNIVERSITY

ANDRIUS KRIŠČIŪNAS

DEVELOPMENT OF HIGHLY CONVERGENT NUMERICAL ALGORITHMS FOR SHORT ELASTIC WAVE SIMULATION

Summary of Doctoral Dissertation
Physical Sciences, Informatics (09P)

2017, Kaunas

This doctoral dissertation was prepared at Kaunas University of Technology, Faculty of Informatics, Department of Applied Informatics during the period of 2012–2017.

Scientific Supervisor:
Prof. Dr. Habil. Rimantas BARAUSKAS (Kaunas University of Technology, Physical Sciences, Informatics – 09P).

Editor: Dovilė Dumbrauskaitė (Publishing Office "Technologija")

Dissertation Defence Board of Informatics Science Field:
Prof. Dr. Habil. Minvydas Kazys RAGULSKIS (Kaunas University of Technology, Physical Sciences, Informatics – 09P) – **chairman**;
Prof. Dr. Habil. Gintautas DZEMYDA (Vilnius University, Physical Sciences, Informatics – 09P);
Prof. Dr. Habil. Rimantas KAČIANAUSKAS (Vilnius Gediminas Technical University, Technological sciences, Mechanical engineering– 09T);
Prof. Dr. Alfonsas MISEVIČIUS (Kaunas University of Technology, Physical Sciences, Informatics – 09P);
Prof. Dr. Miguel A. F. SANJUAN (Rey Juan Carlos University, Physical Sciences, Informatics – 09P).

The official defence of the dissertation will be held at 2 p.m. on 30 August, 2017 at the public meeting of Dissertation Defence Board of Informatics Science Field in the Dissertation Defence Hall at Kaunas University of Technology.

Address: K. Donelaičio St. 73-403, 44249 Kaunas, Lithuania.
Tel. no. (+370) 37 300 042; fax. (+370) 37 324 144; e-mail doktorantura@ktu.lt.

Summary of doctoral dissertation was sent on 28 July, 2017.
The doctoral dissertation is available on the internet http://ktu.edu and at the libraries of Kaunas University of Technology (K. Donelaičio St. 20, Kaunas, Lithuania) and Vytautas Magnus university (K. Donelaičio St. 52, Kaunas, Lithuania).

KAUNO TECHNOLOGIJOS UNIVERSITETAS
VYTAUTO DIDŽIOJO UNIVERSITETAS

ANDRIUS KRIŠČIŪNAS

GREITAI KONVERGUOJANČIŲ SKAITINIŲ ALGORITMŲ SUKŪRIMAS TRUMPŲJŲ BANGŲ TYRIMUI

Daktaro disertacijos santrauka
Fiziniai mokslai, informatika (09P)

2017, Kaunas

Disertacija rengta 2012–2017 metais Kauno technologijos universiteto Informatikos fakulteto Taikomosios informatikos katedroje.

Mokslinis vadovas:
Prof. habil. dr. Rimantas BARAUSKAS (Kauno technologijos universitetas, fiziniai mokslai, informatika – 09P).

Redagavo: Inga Nanartonytė (leidykla „Technologija“)

Informatikos mokslo krypties disertacijos gynimo taryba:
Prof. habil. dr. Minvydas Kazys RAGULSKIS (Kauno technologijos universitetas, fiziniai mokslai, informatika – 09P) – **pirmininkas**;
Prof. habil. dr. Gintautas DZEMYDA (Vilniaus universitetas, fiziniai mokslai, informatika – 09P);
Prof. habil. dr. Rimantas KAČIANAUSKAS (Vilniaus Gedimino technikos universitetas, technologiniai mokslai, mechanikos inžinerija – 09T);
Prof. dr. Alfonsas MISEVIČIUS (Kauno technologijos universitetas, fiziniai mokslai, informatika – 09P)
Prof. dr. Miguel A. F. SANJUAN (Rey Juan Carlos universitetas, fiziniai mokslai, informatika – 09P).

Disertacija bus ginama viešame Informatikos mokslo krypties disertacijos gynimo tarybos posėdyje 2017 m. rugpjūčio 30 d. 14 val. Kauno technologijos universiteto disertacijų gynimo salėje.

Adresas: K. Donelaičio g. 73-403, 44249 Kaunas, Lietuva.
Tel. + 370 37 300 042; faks. + 370 37 324 144; el. paštas doktorantura@ktu.lt.

Disertacijos santrauka išsiųsta 2017 m. liepos 28 d.
Disertaciją galima peržiūrėti internete (http://ktu.edu), Vytauto Didžiojo universiteto (K. Donelaičio g. 52, Kaunas, Lietuva) ir Kauno technologijos universiteto (K. Donelaičio g. 20, Kaunas, Lietuva) bibliotekose.

INTRODUCTION

The simulation of wave propagation in elastic or acoustic media is important in various engineering applications, such as the structural response to dynamic excitation, design and numerical validation of algorithms of ultrasonic measurements, forecasting the extremities of pressure waves and locating the cracks which influence the properties of propagating waves, the simulation of seismic waves traveling through the Earth's layers, etc.

At the first glance, the simulation of such wave propagation processes is simple and straightforward. The propagation of small amplitude waves in elastic or acoustic media is mathematically formulated as linear partial differential equations of continuum mechanics, which can be numerically solved by discretization in space and time. The numerical schemes of wave simulation are based on finite difference method (FDM) or finite element method (FEM) which are well known since 1960–70. Their mathematical principles remained essentially unchanged until now. The numerical wave propagation simulation tools were included into general-purpose FEM software ANSYS, MSC, ABACUS, COMSOL, etc., as well as into specialized wave propagation analysis software WAVE2000 and WAVE3000.

Though mathematically and programmatically simple, numerical wave propagation models still have an inherent "weak spot". They tend to distort the shapes of propagating waves when the space step of the computational grid is too big. The fact that such wave shape distortions may seem physically realistic is disturbing to researchers. Very often they may imitate wave diffractions caused by certain internal inhomogeneity of the media. The general recommendation is that the computational grid intended for the simulation of wave propagation should contain not less than 17–20 finite elements (FE) per wavelength. However, the computation practitioners mostly treat this estimation as strongly non-conservative and choose even denser meshes of ~30 FE per wavelength. An additional disturbance is that the wave of a certain wavelength may generate shorter wave components in the course of propagation and interaction with the media, due to reflection, diffraction and other physical effects. Therefore, the mesh density suitable for simulation of the initial wave may appear as too rough for the wave components appearing in the course of simulation. As a consequence, errors may be produced. Despite different interpretations of the above-mentioned errors as "numerical noises", "diffraction from mesh nodes", etc., they always appear due to too rough computational meshes.

A versatile method for identifying the numerical errors is convergence analysis, where the same physical situation is simulated by using markedly different mesh refinements. However, such approach is costly and problematic, as wave propagation computations are often performed "at the limit" of available computational resources.

Planar shear wave simulation in steel plate of dimensions 10x10cm at frequency 10MHz (ultrasonic waves) can be considered as an example. The wave propagation speed being ~3000 m/s and the wavelength 0.03mm, ~300 wavelengths along the plate must be fitted. The requirement of 20–30 elements along the wavelength may be satisfied by ~0.1mm element size, which results in ~10000x10000 mesh dimensions for this "simple" simulation task. This means that we have 10^8 equations for the acoustic wave, and twice as many for the elastic wave.

Therefore, the most important problem arising in numerical simulations of short wave propagation is a very high demand for computing resources in case waves are short compared to the dimensions of the computational domain. The development of higher order finite elements ensuring the convergence of the solution at 2–3 times rougher grid may reduce the dimensions of the simulation problem by 10–30 times. This work aims to create new highly convergent finite elements for acoustic and elastic wave numerical models.

Research object

The research object is efficient numerical models for high-precision simulations of elastic and acoustic waves, the wavelengths of which are much smaller than the size of the computational wave propagation domain.

Research aim

The aim of the research is to create algorithms for synthesis and to investigate the properties of higher precision order elastic and acoustic continuum finite elements, which may lead to significant reduction of computational resources required for accurate modeling and simulation of short propagating waves.

Research tasks

1. To identify the sources of phase velocity numerical errors in FE models and to analyze the known techniques for their reduction;
2. To synthesize 1D and 2D minimum phase velocity error finite elements with a diagonal mass matrix by applying the synthesis technique of optimally corrected modes
3. To investigate the convergence of wave propagation models based on the synthesized elements in non-homogenous and branched 1D networks;
4. To investigate the convergence of wave propagation models based on the synthesized elements in non-homogenous acoustic and geometrically complex elastic 2D domains;
5. To verify the created finite elements and investigate the advantages and performance of models assembled from the elements in comparison with the models composed of conventional finite elements.

Scientific novelty

A new algorithm based on the modal synthesis approach of optimally corrected modes has been developed in this work. This enabled to obtain the finite element models of significantly broader close-to-accurate modal frequency range compared to earlier models. Although the principal approach to the element synthesis was known before, its main drawback has been overcome in this work. The mass matrices of the new elements are diagonal and can be directly applied in numerical schemes of explicit dynamic analysis.

Practical relevance

Compared to the previously known elements obtained by mode synthesis, the elements created in this work can be directly applied in the explicit dynamics analysis software. The calculations of real objects have been performed by investigating ultrasonic measurement schemes based on the principles of wave propagation.

Approbation of the research results

The main results of the dissertation are represented in six scientific publications: two in the periodical scientific journals (ISI Web of Science) and four in international conference proceedings.

1. FINITE ELEMENT MODELS FOR SHORT WAVE SIMULATION

Two different concepts of dispersion appear by simulating a wave with finite element models (FEM) – mechanical and numerical (Moser, Jacobs, & Qu, 1999). Mechanical dispersion is caused by natural processes, while separate components of a traveling wave move at different velocities, thus the shape of the pulse changes in time. The damping in the model of short wave simulation is usually neglected, therefore mechanical dispersion is non-present in the model. (Ihlenburg & Babuska, 1995). However, the simulation of waves in finite element models always cause numerical errors which impact the traveling pulse similarly to mechanical dispersion. Usually, these errors are called numerical dispersion (**Fig. 1**).

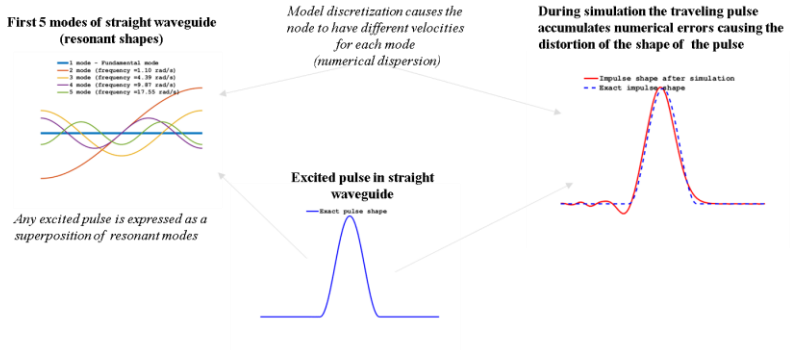

Fig. 1 The representation of numerical dispersion in FE model

Oscillation at any location of the structure of FEM is expressed as a superposition of the model modes. Numerical errors of modes cause different velocity of observed point in a traveling pulse of separate modes, and, depending on the errors of modes, the shape of simulated pulse is slightly distorted in each simulation iteration. In the time-domain simulation, this error tends to accumulate and the distortion of the simulated pulse increases. Usually, these errors are eliminated by using a very dense mesh for FE model, but for short wave simulation this solution causes a huge demand of computational resources.

Typically, in order to reduce the computational resources necessary for wave simulation a thinner mesh model is used; it employs a wider range of close to exact mode frequency of the model obtained by manipulating the FE integration points, using higher order form functions, or the simulation is performed using modified integration schemes. Recently, a number of studies were carried out in this field. It is shown (Yue & Guddati, 2005) that the reduction of numerical dispersion is possible due to the use of the Gauss or Gauss-Labatt integration points for the construction of FE. Better properties of convergence in the model are obtained using generalized mass matrices and non-uniform distances between integration points in FEM, while the Labatt or Chebyshev abscises can be used for optimal solution (Mirbagheri, Nahvi, Parvizian, & Düster, 2015). The minimization of bandwidth of the matrices in 1D higher order element is possible using a template, when several different types of minimization parameters, such as weighting coefficient of different form function or element inner nodes locations, are combined (Khajavi, 2014). When assembling 2D FE models of triangle elements, better convergence is obtained by shifting the element form function integration points from conventional position (Li, He, Zhang, Liu, & Li, 2016). The filtration of numerical errors is possible in additional numerical integration step where numerical dispersion is assessed (Noh & Bathe, 2013). Several studies are based on lumped mass redistribution in the diagonal of higher

order element mass matrix (He, Li, Liu, Li, & Cheng, 2016; Zuo, Li, Zhai, & Xie, 2014).

Another way to reduce the necessary computational resources for wave simulation can be achieved using the mode synthesis technique, where mode synthesis allows a complex structure to be represented with less degree of freedom, d.o.f. (Jie, Xin, & Gangtie, 2015). In most cases, the model is obtained directly from the equations describing the entire model. An attempt to assemble the whole model containing different areas obtained using the mode synthesis technique, leads to poor results. The algorithm presented in Barauskas & Barauskiene, 2004 was proposed to achieve the higher order one-dimensional synthesized 1D finite element by modifying element modes in such way that the number of nodes per unit of wavelength is significantly smaller in comparison to to models of synthesized and conventional elements. Further research in this field is carried out to obtain a synthesized element with similar convergence properties and diagonal mass matrix.

2. THE SYNTHESIS OF THE FINITE ELEMENT

The finite element model of wave propagation in elastic bodies can be presented in the form of general structural dynamic equation system:

$$[\mathbf{M}]\{\ddot{\mathbf{U}}\} + [\mathbf{C}]\{\dot{\mathbf{U}}\} + [\mathbf{K}]\{\mathbf{U}\} = \{\mathbf{F}(t)\}; \quad (1)$$

where $[\mathbf{M}]$, $[\mathbf{C}]$ and $[\mathbf{K}]$ are mass, damping and stiffness matrices, respectively, $\{\mathbf{U}\}$ is the nodal displacement vector and $\{\mathbf{F}(\mathrm{t})\}$ is the excitation force vector.

In the case of small damping, the influence of the damping matrix on the eigenvalues and eigenvectors of the model is also small, therefore we assume that $[\mathbf{C}] = [\mathbf{0}]$ while the element matrices are calculated. Alternatively, small damping can be presented in a proportional form $[\mathbf{C}] = a[\mathbf{M}] + \beta[\mathbf{K}]$, where a, β are coefficients.

Modal frequencies (MF) and modal shapes (MS) of the structure are obtained by solving the eigenvalue problem as:

$$([\mathbf{K}] - \omega^2[\mathbf{M}])\{\mathbf{y}\} = \{0\} \quad (2)$$

where ω – modal frequency, $\{\mathbf{y}\}$ – modal shape.

Real symmetric structural matrices $[\mathbf{M}]$ and $[\mathbf{K}]$ ensure the solutions of (2) as n structural modes $\omega_i, \{\mathbf{y_i}\}, i = 1, \dots, n$. The fundamental properties of structural modes provide that matrices $[\mathbf{M}]$ and $[\mathbf{K}]$ can be expressed in terms of normalized MS and MF as

$$[\mathbf{M}] = ([\mathbf{Y}]^{\mathrm{T}})^{-1}[\mathbf{Y}]^{-1} \quad (3.1)$$

$$[\mathbf{K}] = ([\mathbf{Y}]^{\mathrm{T}})^{-1}[\mathrm{diag}(\omega_1{}^2, \omega_2{}^2, \ldots, \omega_n{}^2)][\mathbf{Y}]^{-1} \tag{3.1}$$

where $[\mathbf{Y}] = [\{\mathbf{y_1}\}, \{\mathbf{y_2}\}, \ldots, \{\mathbf{y_n}\},]$ is the matrix of MS.

This means that the matrices of an element or a structure can be generated by directly referring to the known or desired values of MF and MS. In this case, we knew the first exact MF and MS of the investigated domain, the NDE of the structural model created as (3.1) equals zero for all wave frequencies within the range of the employed MF. However, in most cases it is hardly possible to calculate the necessary number of modes of the whole domain, thus such an approach is of poor practical value. The approach regains practical value in cases when the matrices of the computational domain are assembled of matrices of subdomains which are synthesized by using the appropriate MF and MS. Such subdomains are referred to as synthesized finite elements (SE).

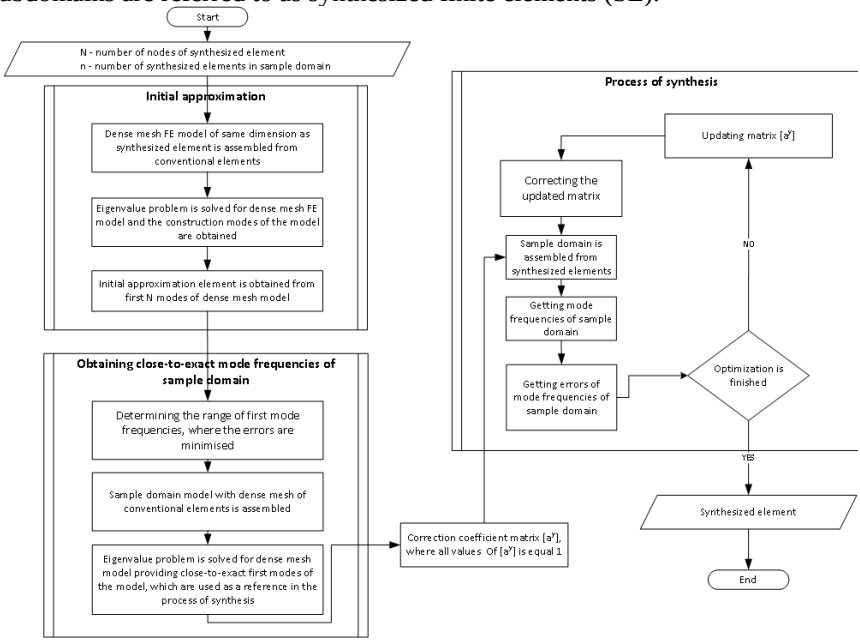

Fig. 2 An outline of the SE generation procedure

The outline of the synthesis procedure of one-dimensional elements is presented in Fig. 2. The computational domain is divided into geometrically simple component substructures (CS) of $\tilde{n}$ d.o.f. each. The external geometrical shape of the CS is the same as of the SE we are going to create. However, the number of d.o.f. of the SE must be much smaller, $n \ll \tilde{n}$. The high mesh refinement of the CS is necessary for ensuring the high accuracy of its first n

modes in case the CS is treated as a stand-alone structure. The matrices of SE are computed by means of relation (3.1), where the first n close-to-exact modes obtained from the highly refined CS model are used. As (3.1) is applied, the MS available in highly refined mesh of the CS are mapped upon much a rougher mesh of the SE in a proper manner. It is worth to mention that for simple geometries of CS the necessary number of its exact modes sometimes can be obtained analytically.

The SE obtained in this way is referred to as the initial approximation element (IAE). By using IAEs, a model of any required geometry could be assembled. Unfortunately, the errors of models assembled of close-to-exact IAEs are significant. Therefore, we enter the optimization loop, where the MS used for the synthesis of SE are treated as optimization parameters. The MS are slightly modified during each optimization loop in order to ensure that a certain reference structure, or sample domain (SD) assembled of a certain number of SEs provides as many as possible close-to-exact modes. At first sight, we could suspect that the result is dependent on the selected size and shape of the SD, which we may select freely. For obtaining the proper modification of the modal shapes, the optimization problem is solved, where 91-noded SD assembled of 10 such SEs is used as a reference structure. It is essential to know the close-to-exact modal shapes of the SD; however, this can be calculated once by using a very dense mesh or sometimes can be obtained analytically. Anyway, the number of d.o.f. N of the SD may be selected much smaller than the number of d.o.f. of the real computational domain of practical value.

The optimization loop in **Fig. 2** is used to minimize the target function which presents the cumulative error of modal frequencies of the SD as:

$$\min_{[\mathbf{a}^y]} \Psi = \sum_{i=1}^{\tilde{N}} \left(\frac{\widehat{\omega}_i - \omega_{i0}}{\omega_{i0}} \right)^2 \tag{4}$$

where ω_i are the MFs of the SD assembled of SE, ω_{i0} are close-to-exact MFs of the SD, and $[a^y]$ is the matrix of MS correction coefficients treated as optimization variables. The summation of errors is performed over $\tilde{N} \leq N$ modal frequencies of the SD.

The correction of MS is performed:

$$[\{\tilde{y}_{11}, \dots, \tilde{y}_{1n}\}, \dots, \{\tilde{y}_{n1}, \dots, \tilde{y}_{1n}\}] = \{\tilde{y}_{11} * a^y_{11}, \dots, \tilde{y}_{1n} * a^y_{1n}\}, \dots, \{\tilde{y}_{n1} * a^y_{n1}, \dots, \tilde{y}_{nn} * a^y_{nn}\} \tag{5}$$

where each j-th term of i-th MS is multiplied by the corresponding value taken from matrix $[\mathbf{a}^y]$. The corrections of all MSs are performed with the exception of the rigid-body modal shapes, which correspond to zero modal frequencies.

The target function (4) is minimized by using the gradient descent method. The gradient $\frac{\delta\Psi}{\delta[\mathbf{a}^y]}$ is expressed as:

$$\delta\Psi = \sum_{\mathrm{i}=1}^{\mathrm{N}} \frac{\widehat{\omega}_{\mathrm{i}} - \widehat{\omega}_{\mathrm{i}0}}{\widehat{\omega}_{\mathrm{i}0}\widehat{\omega}_{\mathrm{i}}} \delta\widehat{\omega}_{\mathrm{i}}{}^2 \tag{6}$$

where

$$\delta\widehat{\omega}_{\mathrm{i}}{}^2 = \{\tilde{\mathbf{y}}_{\mathrm{i}}\}^{\mathrm{T}} \left(\frac{\partial[\widehat{\mathbf{K}}]}{\partial\alpha} - \widehat{\omega}_{\mathrm{i}}{}^2 \frac{\partial[\widehat{\mathbf{M}}]}{\partial\alpha} \right) \{\tilde{y}_{\mathrm{i}}\} \tag{7}$$

As we do not change the mass matrix in order to preserve its diagonal form, $\frac{\partial[\widehat{M}]}{\partial\alpha} = 0$ is assumed. From equations (6) and (7), the gradient $\frac{\delta\Psi}{\delta \mathrm{a}_{\mathrm{ij}}^y}$ is expressed as:

$$\frac{\delta\Psi}{\delta \mathrm{a}_{\mathrm{ij}}^y} = \sum_{\mathrm{i}=1}^{\mathrm{N}} \sum_{j=1}^{N} \frac{\widehat{\omega}_{\mathrm{i}} - \widehat{\omega}_{\mathrm{i}0}}{\widehat{\omega}_{\mathrm{i}0}\widehat{\omega}_{\mathrm{i}}} \{\tilde{y}_{\mathrm{i}}\}^{\mathrm{T}} \left(\frac{\partial[\widehat{\mathbf{K}}]}{\partial \mathrm{a}_{\mathrm{ij}}^y} \right) \{\tilde{y}_{\mathrm{i}}\} \tag{8}$$

where $[\widehat{\mathbf{K}}]$ is assembled in each optimization step of the SE matrices obtained at the previous optimization step.

Derivative $\frac{\partial[\widehat{\mathbf{K}}]}{\partial \mathrm{a}_{\mathrm{ij}}^y}$ is expressed as:

$$\begin{aligned} \frac{\partial[\widehat{\mathbf{K}}]}{\partial \mathrm{a}_{\mathrm{ij}}^y} = -\Big(\{\mathbf{a}^y\}^{\mathrm{T}} [\tilde{\mathbf{Y}}]^{\mathrm{T}} \Big)^{-1} \Big(& [0, \dots, 0, \mathrm{y}_{\mathrm{ij}}, 0, \dots, 0] [\widehat{\mathbf{K}}] [\tilde{\mathbf{Y}}] \{\mathrm{a}^y\} \\ & + \{\mathbf{a}^y\}^{\mathrm{T}} [\tilde{\mathbf{Y}}]^{\mathrm{T}} [\widehat{\mathbf{K}}] [0, \dots, 0, \mathrm{y}_{\mathrm{ij}}, 0, \dots, 0] \Big) \big(\{\mathbf{a}^y\} [\tilde{\mathbf{Y}}] \big)^{-1} \end{aligned} \tag{9}$$

where $[\tilde{\mathbf{Y}}]$ is mode shape of the sample model assembled of SE, y_{ij} – j-th value of i-th mode shape.

2.1 Numerical investigation with application to 1D waveguides

As a numerical example, the analysis of WP in a 1D waveguide is performed. A reference model is assembled of the first order 1D finite elements as:

$$[\mathbf{M}^e] = \frac{\rho A L}{2} \begin{bmatrix} 1 & 0 \\ 0 & 1 \end{bmatrix} \tag{10.1}$$

$$[\mathbf{K}^e] = \frac{EA}{L}\begin{bmatrix} 1 & -1 \\ -1 & 1 \end{bmatrix} \tag{10.1}$$

where A, L – length and cross-sectional area of the element, E, ρ – stiffness modulus and mass density. In 1D case, the exact MF and MS of any straight 1D waveguide can be obtained analytically as:

$$\omega_{i0} = \pi(i-1)/l\sqrt{E/\rho} \tag{11.1}$$

$$y_{i0j} = \sin\left(\frac{2 * pi * (i-1)}{l/(j * L)}\right) \tag{11.1}$$

where i is the mode number, j – number of the component of the i-th MS vector, l – length of the waveguide. The dimensionless results are obtained by assuming $A, E, \rho = 1$. The exact value of the speed of wave is $c = \sqrt{E/\rho} = 1$.

In this numerical experiment IAE is obtained by substituting (11.1) with (3.1), while the MS are mapped on the nodes of the 10-noded SE. Their mass matrix is not changed; it remains diagonal as in the structure of conventional elements, while the corresponding correction of the stiffness matrix is performed as:

$$[\mathbf{K}] = [\mathbf{M}][\mathbf{Y}][\mathrm{diag}(\omega_1, \omega_2, \dots, \omega_n)][\mathbf{Y}]^{\mathrm{T}}[\mathbf{M}] \tag{12}$$

The diagonalization of the mass matrix does not significantly change the MF of the SD, and this work further uses only the diagonal form. However, the obtained IAE introduces much bigger MF errors than would be acceptable.

The stiffness matrix of SE is obtained by minimizing the target function (4). the post-minimization MF errors of the SD are presented in **Fig. 3**, where the error of each MF is presented as computed by $\frac{\hat{\omega}_i - \omega_{i0}}{\omega_{i0}}$. The presented results correspond to different numbers $\tilde{N}$ of MF, the cumulative error of which has been minimized: a) $\tilde{N} = 91$ (100%), b) $\tilde{N} = 63$ (~70%), c) $\tilde{N} = 54$ (~60%). The text henceforth refers to the obtained SE as SE100, SE70, SE60.

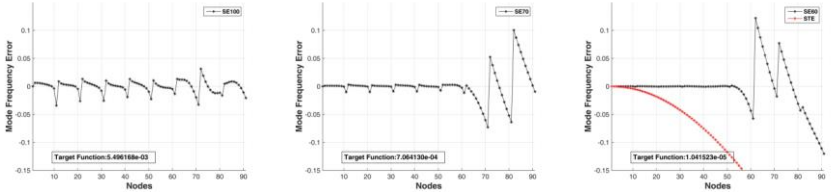

a) b) c)

Fig. 3 Modal frequency errors of the sample domain assembled of 10 synthesized elements at different modal frequencies contributing to the cumulative error: a) 100% (SE100); b) 70% (SE70); c) 60% (SE60);

If the cumulative error minimization is performed over all MFs, $\widetilde{\mathrm{N}} = \mathrm{N}$, the result is rather poor, **Fig. 3a**. However, by selecting smaller values of $\widetilde{\mathrm{N}}$, we may achieve very small values of the cumulative error in this modal range. Perhaps the best result was obtained as $\widetilde{\mathrm{N}}$ comprised 60% of lower MF, where the final target function value read as $\sum_{\mathrm{i}=1}^{\widetilde{\mathrm{N}}} \left(\frac{\hat{\omega}_{\mathrm{i}} - \omega_{\mathrm{i}0}}{\omega_{\mathrm{i}0}}\right)^2 \approx 10^{-5}$. The modal errors of the higher 40% modes seem rather significant, however it is essentially better than could be achieved by using the CFE at the same number of d.o.f., see the red curve of the MF errors in **Fig. 3c**.

A very important property of the investigated models is that the percentage of close-to-exact modes SE does not depend on the overall d.o.f. number of the investigated domain. The frequency value of the higher limit of the close-to-exact MFs range is approximately the same for the stand-alone SE, as well as for the large computational domain assembled of such SE. Therefore, the highest close-to-exact modal frequency value of the SE defines the width of wave spectrum which could be simulated with very small phase velocity errors in waveguide models. **Fig. 4** presents the MF errors of the models of different sizes assembled by using different numbers of nodes as a) $\mathrm{N} = 10$; b) $\mathrm{N} = 361$; c) $\mathrm{N} = 721$. This means that the obtained SE can be used for waveguide structures of different sizes and can be treated as dynamic fast convergence super-element with a diagonal mass matrix.

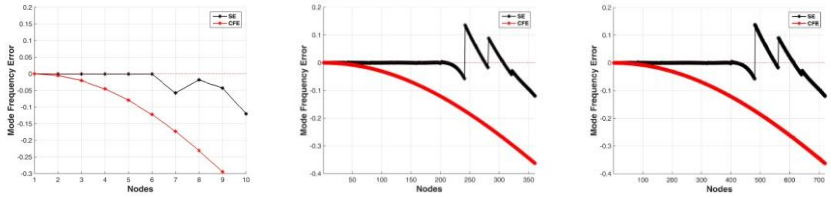

a) b) c)

Fig. 4 The MF errors of models assembled of SE (red) and CFE (black), at different numbers of nodes in the waveguide model: a) N=10; b) N=361; c) N=721;

The synthesis process does not depend on mechanical constants and the obtained element can be used as a template for higher-order synthesized elements, where

$$[\mathbf{K}_{1D}^{SE}] = \frac{EA}{L}[\mathbf{K}_{1D}^{SE0}] \tag{13}$$

Here $[K_{1D}^{SE0}]$ is the stiffness matrix of the synthesized element, $[K_{1D}^{SE}]$ – the synthesized element with real mechanical properties. The mass matrix of the synthesized element is diagonal and identical to the one in the model of conventional elements.

2.2 The procedure of synthesis and numerical investigation with application to 2D models

Generally, synthesis does not depend on the dimensions of the FE model and can be applied to 2D or 3D elements as well as 1D elements. Unfortunately, in higher dimensions, the synthesis procedure becomes very computationally expensive. For example, by comparing 1D and 2D acoustic elements with the same nodes in one direction, the number of optimization parameters in matrix $[a^y]$ increases quadratically. Moreover, it is necessary to obtain the gradients for parameters a_{ij}^y in each optimization step. Thus matrix $[\tilde{K}]$ must be assembled and its dimension increases quadratically as well. Therefore, the number of nodes in synthesized elements of higher dimensions cannot be large. Fig. 5 demonstrates the outline of 2D synthesis procedure.

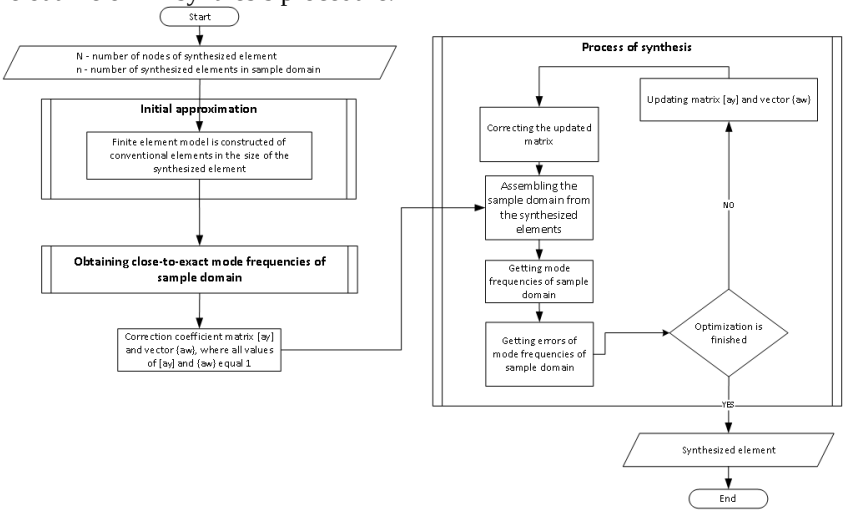

Fig. 5 An outline of the 2D SE generation procedure

In the case of 2D elements, the element is initially constructed of conventional elements. Contrary to 1D, the mode frequencies of IAE are not exact, the correction vector is added to the target function, and, finally, the target function reads as

$$\min_{[\mathbf{a}^y],\{\mathbf{a}^\omega\}} \Psi = \sum_{\mathrm{i}=1}^{\tilde{\mathrm{N}}} \left(\frac{\widehat{\omega}_\mathrm{i} - \omega_{\mathrm{i}0}}{\omega_{\mathrm{i}0}} \right)^2 \tag{14}$$

The calculation of gradient for $[\mathrm{a}^y]$ remains the same as in the case of 1D, while the correction vector $\{\mathrm{a}^\omega\}$ gradients of mode frequencies are expressed analogically as in (6) and (7), where

$$\frac{\delta\Psi}{\delta \mathrm{a}_\mathrm{i}^\omega} = \sum_{i=1}^{N} \frac{\widehat{\omega}_\mathrm{i} - \widehat{\omega}_{\mathrm{i}0}}{\widehat{\omega}_{\mathrm{i}0}\widehat{\omega}_\mathrm{i}} \{\tilde{y}_\mathrm{i}\}^\mathrm{T} \left(\frac{\partial[\widehat{\mathbf{K}}]}{\partial \mathrm{a}_\mathrm{i}^i} \right) \{\tilde{y}_\mathrm{i}\} \tag{15}$$

Here

$$\frac{\partial[\widehat{\mathbf{K}}]}{\partial \mathrm{a}_\mathrm{i}^i} = \left(\{\mathbf{a}^y\}^\mathrm{T} [\tilde{\mathbf{Y}}]^\mathrm{T} \right)^{-1} (diag[0, \dots, 0, \omega_i^2, 0, \dots, 0]) \left(\{\mathbf{a}^y\} [\tilde{\mathbf{Y}}] \right)^{-1} \tag{16}$$

The element matrix of conventional 2D acoustic elements reads as

$$[\mathbf{M}^e] = \frac{\rho * S^e}{4} [\mathbf{I}] \tag{17.1}$$

$$[\mathbf{K}^e] = \rho \int_{Ve} ([\mathbf{B}])^T [\mathbf{D}] \, [\mathbf{B}] \mathrm{d}V = E * S^e [\mathbf{B}]^T [\mathbf{B}] \tag{17.2}$$

where S^e – area of element, $[\mathbf{I}]$ and $[\mathbf{B}]$ – unit and geometry matrices, $[D]$ – stress matrix, which is diagonal in the acoustic case, where diagonal elements are equal to the Young modulus of the material.

Additional difference in the 2D case is the existence of symmetric modes with same mode frequency, where their correction coefficients can be calculated for one of them, while the other mode is obtained with:

$$\{\tilde{\mathbf{y}}_{\mathrm{s}2}\} = [\mathbf{T}]\{\tilde{\mathbf{y}}_{\mathrm{s}1}\} \tag{18.1}$$

$$\tilde{\omega}_{s2} = \tilde{\omega}_{s1} \tag{18.2}$$

where s1, s2 – numbers of symmetric modes, $[\mathbf{T}]$ rotation of 90° matrix.

Square elements with 5×5 nodes are used for the construction of 2D synthesized finite element. The process of synthesis should minimize the errors of the first 25% of mode frequencies of the sample domain assembled of 25 elements.. The results of synthesis are provided in **Fig. 6**a.

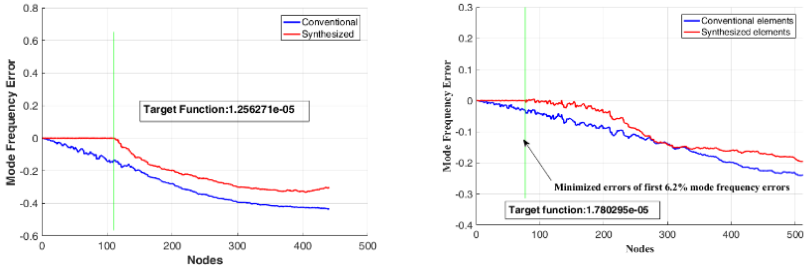

a) b)

Fig. 6 . Mode frequency errors of a) the acoustic model b) the elastic model

The value of target function after synthesis is $\sum_{i=1}^{\tilde{N}} \left(\frac{\tilde{\omega}_i - \omega_{i0}}{\omega_{i0}}\right)^2 \approx 1.26 * 10^{-5}$ (**Fig. 6a**) which is close to the results obtained of 1D elements. Additionally, the stiffness matrix of the synthesized element can be used as a template for the construction of synthesized elements with different mechanical properties:

$$[\mathbf{K}_{2D}^{SE}] = E * [\mathbf{K}_{2D}^{SE0}] \tag{19}$$

The mass matrix of models assembled of the synthesized elements remains diagonal and identical to the one in the model of a conventional element.

the main difference created by the process of elastic wave synthesis is that the stress matrix reads as:

$$[D] = \frac{E}{(1+\upsilon) * (1-2\upsilon)} \begin{bmatrix} 1-\upsilon & \upsilon & 0 \\ \upsilon & 1-\upsilon & 0 \\ 0 & 0 & (1-2*\upsilon)/2 \end{bmatrix} \tag{20}$$

where υ is Poisson's ratio. Similarly to cases of 1D and 2D acoustic FE models, the close-to-exact mode frequencies in the elastic FE model can be obtained by solving the eigenvalue problem for the same structure but with a much finer FE mesh. While the modes of 1D and 2D acoustic FE models do not depend on mechanical properties, the mode frequencies and mode shapes in 2D elastic elements depend on Poisons ratio. It means that the synthesized elastic elements cannot be reused as a template for the materials with different Poison's ratio, and the synthesis for each material should be performed separately. Moreover, there are 2 d.o.f. in each node in the elastic model and the matrices used in the process of synthesis are 2 times bigger when compared with acoustic 2D models. Hence, 4×4 nodes square element has been selected for the construction of a 2D elastic synthesized finite element. During synthesis, the errors of the first 6.2% mode frequencies of the sample domain assembled of 25 elements are minimized. The

results of synthesis are shown in **Fig. 6**b (aluminum – Poison's ratio $\upsilon = 0{,}3435$). After synthesis, the target function value is close to $1.8 * 10^{-5}$ and is of the same order as in 1D or 2D acoustic cases.

3. CONVERGENCE INVESTIGATION OF MODELS ASSMEBLED OF SYNTHESIZED ELEMENTS

3.1 Numerical investigation with application to wave simulation in 1D waveguide

It is considered that the wave pulse is excited at the left-hand end of the 1D waveguide structure and propagates along it. Theoretically, the pulse should move along the structure at the speed of sound, without changing its form. In order to evaluate the extent of deterioration of the pulse shape due to numerical dispersion errors the following simulation quality indicators are used: wave amplitude a_m at the peak of wave; maximum value of numerical noise (NN) a_n and the width a_l of the pulse at its height $\frac{\sqrt{2}}{2} * a_m$ (**Fig. 7**). In the case of exact solution, we have $a_n = 0$, $a_m = 1$.

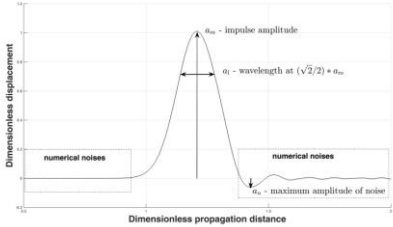

Fig. 7. A graphical interpretation of simulation quality indicators $\boldsymbol{a_n}$, $\boldsymbol{a_l}$ and $\boldsymbol{a_m}$

Assume that the straight 1D structure is assembled of 20 SE, where the length of each element $l_e = 0.1$, total length of the structure $l = 2$, total number of nodes $N = 181$, the distance between adjacent nodes $L = \frac{l_e}{10-1} \approx 0{,}011$. The dimensionless wave speed is c= 1. The simulation is performed during time period $T = 7\ (s)$, while the distance travelled by the pulse is $S = 7$. The obtained results are compared against the results obtained in the CFE model of the same dimensionality and against the results obtained in a very dense (90 nodes per wavelength) CFE mesh. The latter has been regarded as the close-to-exact solution. The wave simulation is performed by actuating the displacement at the left-hand end of the waveguide as:

$$u(t) = \begin{cases} (1 - \cos(\frac{\pi}{deltaT} t)) * deltaU, & t < deltaT \\ 0, & t \geq deltaT \end{cases} \quad (21)$$

where $deltaT$ is the actuation time, $deltaU$ is the wave amplitude. The dimensionless results are obtained by assuming $deltaU = 1$. A comparison of the results at different space-steps of the model is presented in **Fig. 8**, where the propagation distance is expressed in terms of the length of the wave pulse.

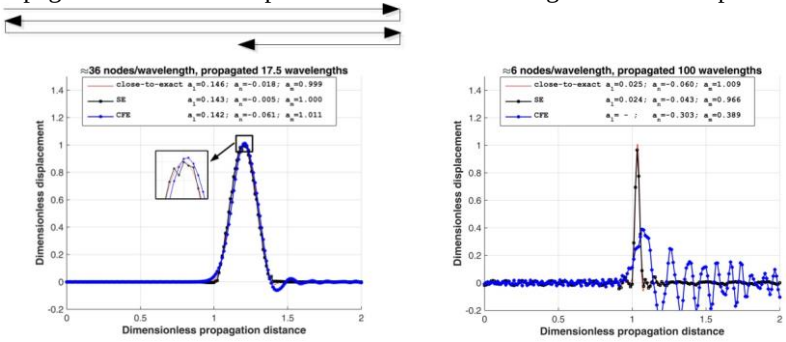

a) b)

Fig. 8. Simulation results after 7 s: a) $\mathbf{deltaT = 0.4}$, 36 nodes per wavelength, pulse propagated 17.5 wavelengths; d) $\mathbf{deltaT = 0.07}$, ≈6 nodes per wavelength, pulse propagated 100 wavelengths;

In all cases, the accuracy of the model assembled of SE is the best with less than 10% of errors compared against the models of conventional elements. Even 6 nodes per pulse-length in the model assembled of SE produce reasonable simulation results which are impossible to achieve by using conventional elements at the same mesh density, **Fig. 8b**. Attention should be drawn to the small distortion of the pulse shape at the peak of the pulse as SE with a dense mesh (36 nodes per wavelength) were used, **Fig. 8a**. Apparently, it is a consequence of the lower MS correction, which is performed as the element is synthesized. This imperfection exhibits itself at the moment of excitation of the pulse as the mesh is dense. However, the distortion disappears when a combined model assembled of conventional FE and SE is employed (**Fig. 9**). The explanation is as follows. Both conventional FE and SE meshes ensure the close-to-exact MF values, therefore the propagation speed of all harmonic components of the pulse is represented correctly. The representation of the pulse shape depends on MS which are a little distorted in SE. As the pulse comes back to the segment presented by CFE, the distortion of the pulse shape disappears. Practically, this distortion is very small because the corrections of the lower MS of the SE are small.

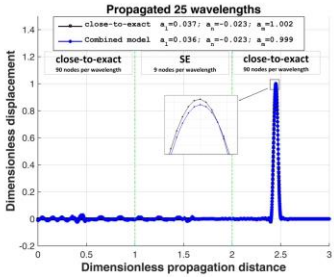

Fig. 9. Wave propagation in the combined model assembled of SE60 and STE

The wave-pulse propagation in a branchy non-homogenous model assembled of SE has been investigated in a sample model with 3 waveguide segments of different properties. The diameters of circular cross-sections are $D_1 = 0.1$, $D_2 = 0.08$ and $D_3 = 0.05$, mass densities $\rho_1 = 0.8$, $\rho_2 = 1.2$, $\rho_3 = 1$, bulk moduli and lengths are $K_{1,2,3} = 1$ and $L_{1,2,3} = 1$. Depending on mass densities, the speeds of the wave are $C_1 \approx 1.12$, $C_2 \approx 0.91$, $C_3 = 1$. The geometry of the investigated domain is presented in **Fig. 10**a.

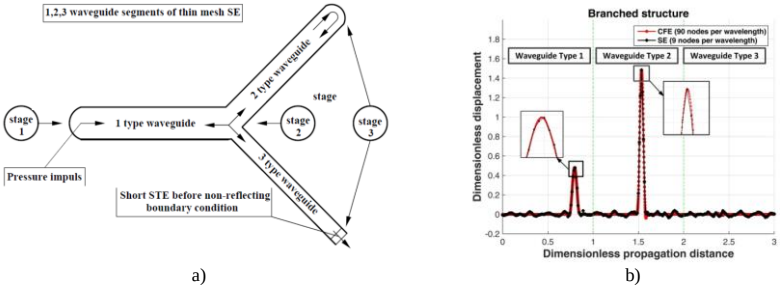

a) b)

Fig. 10 a) The geometry of a branched non-homogenous structure **b)** Simulation results after 2.55 (s)

Simulation starts by actuating the wave pulse as (13) at the left-hand end of segment 1, where deltaT = 0.1 (s), deltaU = 1 (**Fig. 10a**, stage 1). After ~1 (s), the wave-pulse reaches branching, is partially reflected back and partially continues through segments 2 and 3 (**Fig. 10a**, stage 2). After ~2 s, the pulse is reflected from the end of segment 2 and comes back, while the non-reflecting boundary condition is implemented at the end of segment 3 (**Fig. 10a**, stage 3) as:

$$\sqrt{\frac{K}{\rho}}\frac{\delta u}{\delta x} + \frac{\delta u}{\delta t} = 0 \tag{22}$$

Two models were created for the analysis of wave-pulse propagation in a branchy non-homogenous structure. The model assembled of SE contained ~9 elements per pulse-length, and the model assembled of CFE contained ~90 nodes per pulse-length (close-to-exact solution). The exact number of nodes per pulse-length depends on the mechanical properties of a particular segment. The non-reflecting boundary condition cannot be implemented in SE directly; therefore, a short CFE was joined at the end of segment 3 where the non-reflecting boundary condition can be adequately implemented. Simulation results after 2.55 s at the end of stage 3 in **Fig. 10a** are presented in **Fig. 10b**. It can be concluded that only negligible discrepancies could be observed compared with the reference model, though the SE60-based model was employed in a quite general and combined situation. The discrepancy between the two models could be estimated as 0.04 relative level numerical noise, which was observed in the SE60-based model.

Error of estimation e_ω is used In order to investigate the influence of the number of nodes per pulse length on the accuracy of wave simulation results, where the models are assembled of SE or of CFE,. Assume the wave pulse (21) is actuated in the waveguide of length $= 2$, where the actuation time is $deltaT = 0.1\ (s)$ and the dimensionless wave propagation speed is $C = 1$ (m/s). The width of the Fourier spectrum defines the frequency range in which the modal frequencies of the model should be close-to-exact in order to provide accurate simulation results. This enables to approximately predict the magnitude of the propagating wave-pulse simulation error in terms of modal frequency errors of the finite element structure.

In the case of 1D straight beam, the modal frequencies coincide with the frequencies of the harmonic components of the Fourier spectrum. The error of representation of the propagating wave pulse can be evaluated as:

$$e_\omega = \sum_{1}^{\mathrm{N}} f_i \left(\frac{\widehat{\omega}_{\mathrm{i}} - \widehat{\omega}_{\mathrm{i0}}}{\widehat{\omega}_{\mathrm{i0}}} \right)^2 \qquad (23)$$

where f_i is the amplitude of the component of i-th frequency of the Fourier spectrum, $\left(\frac{\widehat{\omega}_{\mathrm{i}} - \widehat{\omega}_{\mathrm{i0}}}{\widehat{\omega}_{\mathrm{i0}}}\right)^2$ – relative error of i-th modal frequency of the structure. The magnitude of e_ω allows to evaluate the amount of distortion of the wave pulse shape. The evaluation is approximate since during the simulation the wave pulse spectrum slightly changes due to the generated numerical noises.

Assume that if e_ω is equal for two different models, their abilities to correctly represent the shape of the propagating wave pulse are the same. Rrrors e_ω of models assembled of SE and of CFE are compared in **Fig. 11a** , while different number of nodes of the models is used: $100 \leq \mathrm{N} \leq 1100$.

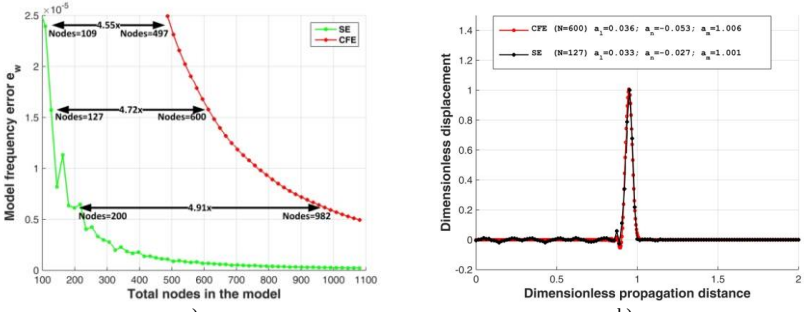

a) b)

Fig. 11 A comparison of the $\boldsymbol{e_\omega}$ values of the SE60 and CFE models assembled against their number of nodes (a) and a comparison of the shapes of the simulated wave pulse in the SE60 and CFE models at node numbers $\boldsymbol{N_{SE60} = 127}$ and $\boldsymbol{N_{CFE} = 600}$ (equal values of $\boldsymbol{e_\omega}$ in both models) (b)

Fig. 11a demonstrates that e_ω value of the CFE model is same as e_ω value of the SE model with more than 4.5 times rougher mesh. The performance of the SE model in wave pulse simulation is demonstrated in **Fig. 11b**, where very similar results were obtained by using the CFE model containing $N_{CFE} = 600$ nodes and by using ~4.7 times rougher SE model containing only $N_{SE60} = 127$ nodes. The obtained indicator a_l, a_n and a_m values of simulation quality differ by less than 1% between the two models. However, the number of non-zero positions in the matrices of the SE model is larger, as the bandwidth of SE model matrices is equal to the number of nodes of a single SE, while the bandwidth of matrices assembled of CFE is always 3 and there are not enough to compare models by using only mesh roughness criteria. The actual evaluation of the computational resource used for wave simulations includes the amount of memory and the number of operations, which should by performed during each numerical integration step by employing the central difference numerical integration scheme. Considering that the SE60 matrices are assumed to be known in advance, in order to investigate the usage of computational resources, numerical experiment of ultrasonic longitudinal wave propagation in 1D aluminum waveguide is performed, where computational times are compared for models assembled of CE and SE60 with 4.7 rougher mesh (30 nodes per wavelength in model of CE and 6.36 in model of SE, respectively). Simulation is performed while pulse propagates the whole waveguide, thus total time of simulation increases by increasing the length of the waveguide. The experiment is performed using Matlab R2015a with sparse mass and stiffness matrices on a machine with Intel Core i7-4790 CPU @ 3.60 Hz processor, 32GB RAM and 64-bit Windows Operating System. Physical constants of the FE model waveguide of equation (10) are $E = 71.788$ MPa, $\rho = 2780\ \mathrm{kg/m^3}$, wave speed $5081\ \mathrm{m/s}$, pulse actuation time

40 μs and the integration step is 0.4 μs. Results which show the influence of total number of simulation steps and computational time on the length of the waveguide are presented in **Table 2**.

Table 1 A comparison of computational times using FE models assembled of CE and SE60

Length (m)	Simulation time (ms)	Total steps	Model of CE		Model of SE60		Improvement (%)
			Nodes	Computational time (s)	Nodes	Computational time (s)	
10	1.97	4,920	1,476	0.158	316	0.083	47
20	3.94	9,839	2,952	0.551	622	0.305	45
50	9.84	24,598	7,380	3.366	1,567	1.571	53
100	19.68	49,197	14,759	13.607	3,124	6.907	49
200	39.58	98,394	29,518	56.966	6,256	23.982	58

Results in Table 1 show that the improvement of computational time obtained by performing the simulation is larger when compared with the results obtained by calculating arithmetical operations. An additional advantage of the SE models is a larger value of the limit time step ensuring the stability of the numerical integration scheme.

3.2 Numerical investigation with application to 2D acoustic wave propagation

A rectangle of 500×200 m with non-dimensional mechanical properties $E = 1$ and $\rho = 1$ and wave speed of $C = 1\mathrm{m/s}$ is used to perform the investigation of wave propagation in 2D acoustic models assembled of synthesized and conventional elements **(Fig. 12**).

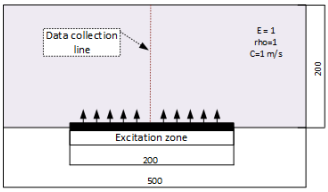

Fig. 12 The geometry of the 2D model

Impulse (21) is excited for 100 s. Two equal density mesh (L=10) models are assembled of CFE and SE, and one close–to-exact (5 times denser mesh, L=0.2) model of CFE is assembled. Simulation results with different pulse excitation times in the models are provided in **Fig. 13**.

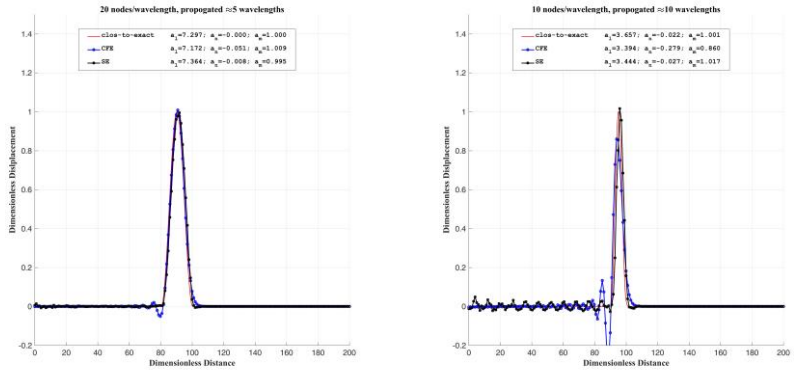

a) b)

Fig. 13 A comparison of simulation results after 100 s a) deltaT = 20, 20 nodes per wavelength; b) deltaT = 10, 10 nodes per wavelength

Fig. 13 demonstrates the values of the quality indicators a_n, a_l and a_m of the simulated pulse in 2D acoustic model at data collection line, while different nodes per wavelength are used. The results show that all indicators are close–to-exact in the model of SE with 10 nodes per wavelength, while in model of CFE, similar results are obtained with 20 nodes per wavelength. To obtain a more accurate comparison based on mesh density in different models, 2D Fourier transformation is performed for the simulation results obtained at the time at data collection (B-scan image) by converting the results from displacement–time space to the phase velocity–frequency space. The obtained dispersion curves are shown in **Fig. 14**.

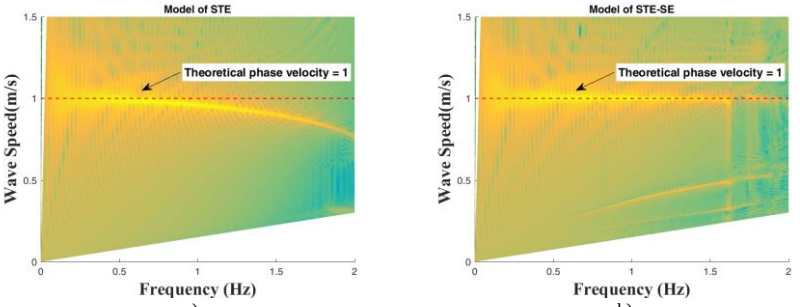

a) b)

Fig. 14 Dispersion curves of the 2D model obtained from the simulation results

Theoretical wave speed in the mode is 1 m/s. Dispersion curves show that in CFE models, close to theoretical phase velocity is achieved until ~0,65Hz, while in SE models - until ~1,6Hz. This means that the mesh of the SE model can be

~2.5 times coarser when compared with the CFE model. **Fig. 15** demonstrates the simulation results at data collection line in the twice larger construction (1000x400) as a B-scan image, while pulse is simulated in the SE and CFE models with identical mesh (**Fig. 15**a,b) and with 2.5 times denser mesh in the CFE model (**Fig. 15**c). The simulation lasted 360 s.

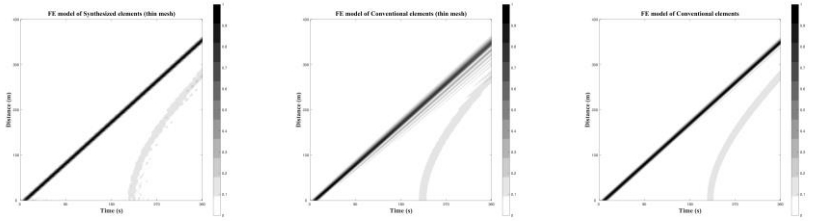

a) b) c)

Fig. 15 B-Scan images of simulated pulse in a and b) SE and CFE models with same density; c) CFE models with 2.5 times denser mesh

Simulation results show some similarities in models of SE and CFE with 2.5 denser mesh. On the other hand, in the CFE model with the same mesh density as in SE model noises cause numerical dispersion to mingle with the pulse reflection from the model walls.

To compare the SE and CFE models in the computational resource manner, SE and CFE with 2.5 denser mesh models are compared. Monitoring indicators are the degrees of freedom in models, memory necessary in simulation for keeping the vectors $\{\ddot{U}\}, \{\dot{U}\}$, $\{U\}$ and sparse symmetric matrices [K], [M], and the computational time. The comparison is performed by constructing quadratic shape models and simulating the pulse passing through the model and gradually increasing the model edge length (**Fig. 16**a). Wave speed in the model is 1m/s, and the integration step 0.01s. The results of indicators provided in **Fig. 16**.

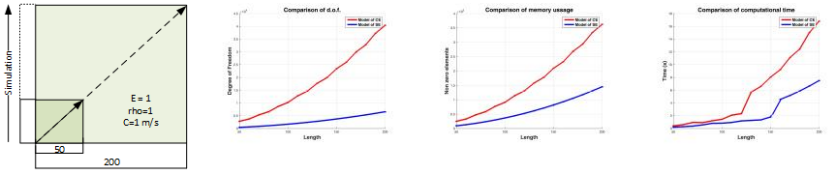

a) b) c) d)

Fig. 16 A comparison of FE models assembled of SE and SFE a) graphical comparison interpretation b) comparison of d.o.f; c) comparison of memory; d) comparison of computational time

The results of comparison in **Fig. 16** show that the model assembled of SE is better on all compared indicators. The d.o.f number can be ~6 time lesser in the model made of CFE compared with the SE model, while memory computational time required for pulse simulation is ~2.3 times lesser.

3.3 Numerical investigation with application to 2D elastic wave propagation

The verification of 2D elastic synthesized elements is performed by simulating a pulse in a 0.384 x 0.64 m rectangle (**Fig. 17**) using aluminum (mechanical properties $E = 70GPa$ and $\rho = 2700\,kg/m^2$).

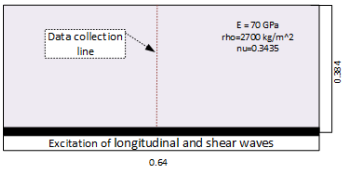

Fig. 17. The geometry of elastic FE model

Simulation of the pulse is performed by exciting the pulse for $dT = 4\mu s$ and performing the simulation for $T = 50\mu s$, while the amplitude of the pulse is $dU = 1 \times 10^{-11}$. After the simulation, reflections from the geometry wall do not arrive to the data collection line, and the impulse form should be the same as excited pulse. Simulation results in models of different SE and SFE meshes are provided in **Fig. 18**, where the length of the square element edge is 2, 1 and 0.5 mm. Respectively, the number of degrees of freedom in such models is about 127,000; 492,000 and 1,971,000.

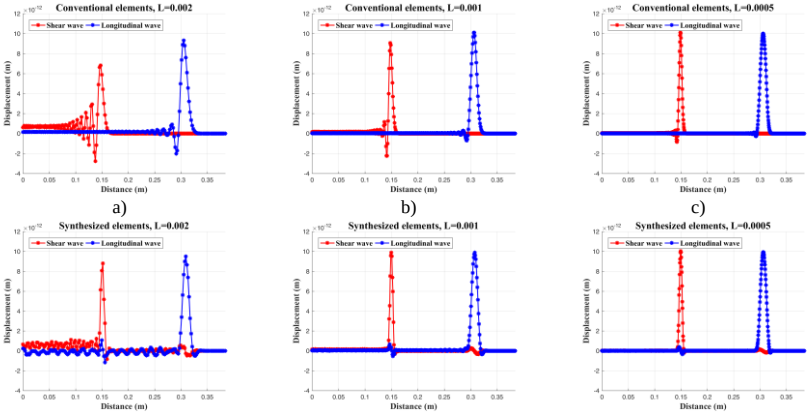

a) b) c)

d) e) f)

Fig. 18 The convergence investigation of pulse propagation in 2D elastic FE model with different mesh a, b, c) models assembled of conventional elements; c, d, e) models assembled of synthesized elements

Simulation results show that numerical errors in SE models are smaller compared with such errors in CFE models. In order to obtain results similar to the ones for the CFE model with element edge length of 0.5 mm, the element edge length in the SE model can be 1 mm. It also should be noted that propagating shear and longitudinal waves in the SE model generates small errors (~2% of impulse amplitude) for other types of waves. These errors may be caused by the correction of modes in the process of synthesis, and are not eliminated by using a dense mesh (**Fig. 18**f). However, the locations of these errors are predictable and they can be easily eliminated during post-processing. The dispersion curves obtained from B-scans after 2D Fourier transformation are given in **Fig. 19**.

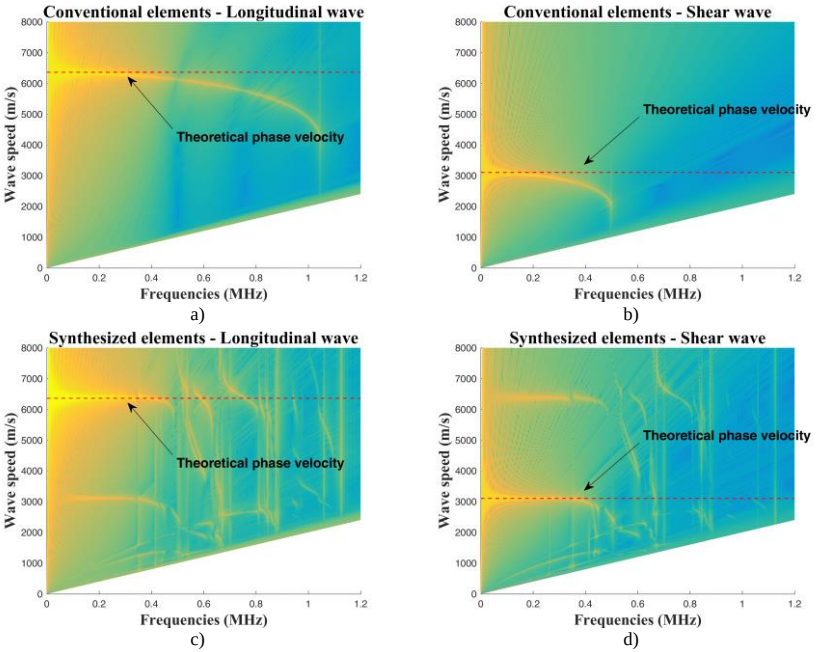

Fig. 20 Dispersion curves of 2D elastic model obtained from the simulation results

The dispersion curves **(Fig. 20**) indicate that the range of close–to-exact frequencies in SE model is the same for both longitudinal and shear waves, while in the SFE model they differ. By taking into account that the range of mode frequencies in a model should be close to exact for waves of both types, the SE

model with a 2 times wider frequency range can be simulated using the same mesh refinement as compared with the CFE model (SE ~0.4MHz; SFE ~0.2 MHz); or, respectively, the SE model can be assembled with 2 times rougher mesh compared with CFE. **Fig. 21** demonstrates model performance indicators where the same experiments as in 2D acoustic case are performed for 2D elastic models assembled of SE and CFE with 2 times rougher mesh.

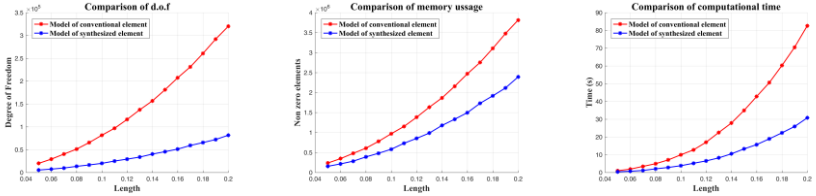

a) b) c)

Fig. 21. A comparison of elastic 2D FE models assembled of SE and SFE a) a comparison of d.o.f; c) a comparison of memory; d) a comparison of computational time

The results show that usage of relatively small elastic synthesized element (4x4 nodes; 10 nodes element was created for 1D case) allows to decrease memory usage by ~1.5 times and computational time by ~3 times for wave simulation.

4. NUMERICAL EXPERIMENTS

4.1 Fluid transient analysis in one-dimensional branched non-homogenous environment

The equations (21) cannot be directly applied for the simulation of pressure pulse in pipelines of flowing fluid. Therefore, pressure pulse analysis equivalent of fluid bulk modulus is used which considers fluid compressibility and the elasticity of pipelines vessel walls:

$$\widetilde{K} = K(1 + \frac{KD}{hE})^{-1} \tag{24}$$

Here K – fluid bulk modulus; D – diameter of the pipeline; E – Young's modulus of pipeline; h – width of pipeline vessel wall. In the case of steady flow analysis, the stiffness matrix of an element is expressed as:

$$[\mathbf{K}_T^e] = \sqrt{\frac{D}{2fL|C|}\left(A^2\rho - \frac{w_e^2}{\widetilde{K}}\right)}\begin{bmatrix} 1 & -1 \\ -1 & 1 \end{bmatrix} \tag{25}$$

Here $f = \frac{0.3614}{RE}$ – friction, where $RE = \frac{\rho D|v|}{\mu}$ is Reynold's number (μ-dynamic viscosity fluid, ρ – density fluid). In order to find steady flow results, the debit values are renewed in each Newton-Raphson iteration: $w_e^{(n)} = w_i^{(n-1)}$(here n is the number of iteration). After Newton-Raphson iterations, the transient simulation should also be performed without additional stimulus. Damping will cause the model to reach a steady state when debits and pressures are consistent. Such a steady state can be used as an initial condition for transient simulation with a stimulus described by:

$$\begin{cases} [\mathbf{M}^e]\{\ddot{\mathbf{p}}^e\} + \left[\mathbf{C}^e\left(\dot{\mathbf{P}}^e, \mathbf{P}^e\right)\right]\{\dot{\mathbf{P}}^e\} + [\mathbf{K}^e(\mathbf{P}^e)]\{\mathbf{P}^e\} + \{\mathbf{Q}^e\} = 0 & (26.1) \\ \dot{v}_e = G & (26.2) \end{cases}$$

Here$\{P^e\}$ is the pressure vector, $\{\mathbf{Q}^e\}$ – external force vector. Other matrices and vectors from (26) can be found with:

$$[\mathbf{M}^e] = \frac{AL}{2}\begin{bmatrix} 1 & 0 \\ 0 & 1 \end{bmatrix} \quad (27.1)$$

$$[\mathbf{C}^e] = \frac{ALf|v_e|}{2D}\begin{bmatrix} 1 & 0 \\ 0 & 1 \end{bmatrix} \quad (27.2)$$

$$[\mathbf{K}^e] = \frac{A\widetilde{K}}{L}\begin{bmatrix} 1 & -1 \\ -1 & 1 \end{bmatrix} \quad (27.3)$$

$$\{\mathbf{Q}^e\} = A\widetilde{K}\left(\frac{p^*}{L} - \frac{f v_e|v_e|}{2D} - g\sin a\right)\begin{Bmatrix} 1 \\ -1 \end{Bmatrix} \quad (27.4)$$

$$G^e = \frac{v_e}{\widetilde{K}}\frac{\dot{p}_1 + \dot{p}_2}{2} - \frac{p_2 - p_1}{\rho_0 L} - \frac{f}{D}\frac{v_e|v_e|}{2} - g\sin a^2 \quad (27.5)$$

here v – the velocity of fluid flow, a – the angle the pipeline makes with a horizontal line, g – the free-fall acceleration. The first equation of system (26) is transformed into the equation describing the whole system, while the second one is solved for each element separately. The non-reflection condition of the wave can be expressed as:

$$\sqrt{\frac{\widetilde{K}}{\rho}}\frac{\delta p}{\delta x} + \frac{\delta p}{\delta t} = 0 \quad (28)$$

Equation (28) fully meets equation (23) which was investigated while convergence analysis was performed in the models of synthesized and conventional elements in branched non-homogenous structure. The main difference of the previous investigation is that here damping appears, which depends on the mechanical properties of the pipeline and fluid as well as the flow speed in the model. To create the SE for fluid transient analysis in one-dimensional

branched non-homogenous environment, SE stiffness matrix for steady flow and dynamic analysis are expressed as:

$$[\mathbf{K}_T^e] = \sqrt{\frac{D}{2fL|C|}\left(A^2\rho - \frac{w_e^2}{\widetilde{K}}\right)}[\mathrm{K}_{1D}^{SE0}] \tag{29}$$

$$[\mathbf{K}^e] = \frac{A\widetilde{K}}{L}[\mathbf{K}_{1D}^{SE0}]$$

A branched non-homogenous structure is assembled of SE and CFE for verification of the SE (**Fig. 22**).

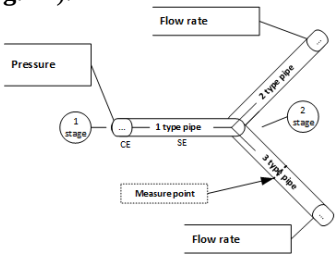

Fig. 22. A branched non-homogenous structure

In the numerical experiment, a sample construction assembled of segments used in thermal pipelines is analyzed, where the mechanical properties of pipelines are $E = 2.1 \cdot 10^{11}$, $K = 2.2 * 10^9$, $\rho = 995$, $\mu = 0.045 \cdot 10^{-3}$, diameters and thickness of walls of pipelines are, respectively, $D_1 = 0.1$, $D_2 = 0.08$, $D_3 = 0.1$ and $h_1 = 0.0035$, $h_2 = 0.003$, $h_3 = 0.0025$. As an initial condition, pressure $P = 4 * 10^5 Pa$ is selected for the beginning of type 1 pipe, while for type 2 and type 3 pipes, flow debits are set to $w_{1,2} = 10\, m^2/h$ at the end of the pipe. The length of each segment is $L_s = 4000m$. The synthesized elements in this case have 10 nodes, thus flow velocity by (26.2) is obtained in the whole element in the SE model, while in the CFE model it can be found between nodes. The results of steady flow analysis are shown in **Fig. 23**, where the length between nodes is $L \approx 24.7m$.

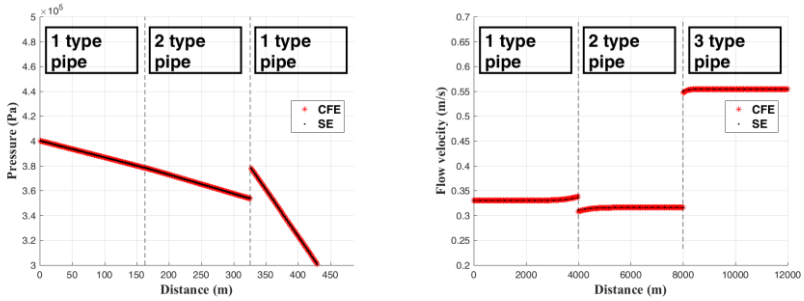

a) b)

Fig. 23 Results of steady flow analysis in a branched non-homogenous structure: a) pressures b) flow velocities

Simplification in simulation is made: it is accepted that flow velocity does not change in time and $\acute{v}_e = 0$. The simulation starts by actuating the (21) pulse by $dT = 0.2s$ of amplitude $dP = 1 \cdot 10^5 Pa$ in the left of type 1 pipe. A comparison of the resulting pressure pulses after simulation in different models is shown in **Fig. 24**a (there are 11 nodes per wavelength and pulse is propagated by ~23 wave lengths).

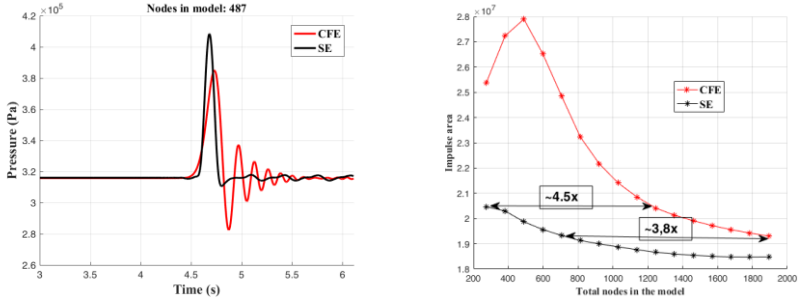

a) b)

Fig. 24 a) Pressure value of pulse in measurement point observed in time b) Comparison of models by mesh roughness

Simulation results in **Fig. 24**a show that the model using CFE results in numerical noise (the "wavy" region after the pulse) with maximal amplitude being almost half amplitude of the original front pulse. On the other hand, similar noises in the SE model are insignificant.

Pulse simulation in SE and CFE models using different meshes is compared in **Fig. 24**b. The area formed by propagating pulse in time interval from 4 to 4.5 in measurement point is assessed by:

$$e_i = \sqrt{\frac{t_{min}}{T} \sum_{i=0}^{T/t_{min}} \left(\sqrt{P(i * t_{min}) - P_p} \right)^2} \tag{30}$$

where, t_{min} – numerical integration step, P_p – pressure value at point after steady flow analysis, $P(i * t_{min})$ – pressure value in the point at specific time. The results show that depending on desired accuracy, convergence of the model of SE is much better (3.8–4.5 times), and the improvement is similar to the one which was obtained by previous comparison (**Fig. 11a**), when the mode frequencies errors and the pulse frequency spectrum was combined as an indicator to compare the models of different elements.

4.2 Calculation of ultrasonic measurement in acoustic non-homogenous environment

A non-homogenous 2D rectangle 0.64 x 0.24 m structure has been selected to verify the use of synthesized elements by performing simulation of ultrasonic measurements. Two FE models with the same mesh refinement are assembled of squared 0.5 x 0.5 mm SE and CFE. CFE matrices are obtained from (17). For SE, the mass matrix is obtained from (17.1), while a 5x5 nodes template was used for the stiffness matrix, obtained in the synthesis process (19) was used. The geometry of the model is shown in **Fig. 25**.

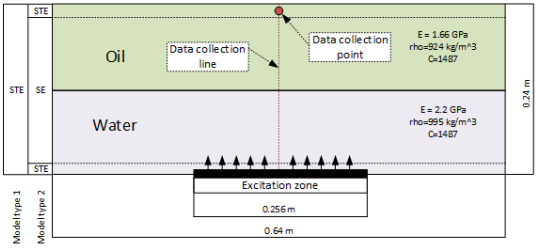

Fig. 25 A geometry of a 2D non-homogenous FE model

Gaussian window pulse is excited in water ($E = 2.15$ GPa, $E = 999.8$ kg/m^2, $C = 1466$ m/s) for 10 μs. The traveling pulse partially reflected passes to the oil environment ($E = 1.35$ GPa, $E = 920$ kg/m^2, $C = 1211$ m/s).

Damping in the model is neglected, and there are no reflections from walls or inhomogeneities. Thus, the shape of the traveling pulse in time should not change. The simulation results are provided as a B-scan image of results collected in time in data collection line (**Fig. 26**).

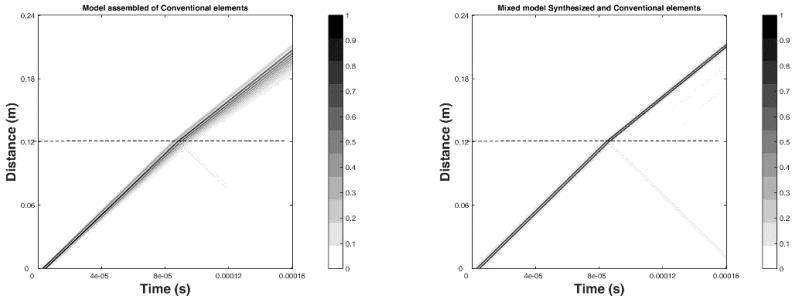

a) b)

Fig. 26 B-Scan images of simulated pulse in models of a) CFE b) SE and CFE combination

By comparing the results in same mesh refinement models of SE and SFE, it is seen that, in the SE model, reflections appear only when the pulse crosses between different materials, while in the CFE model, the distortion of pulse grows while it travels in the same material and the reflected pulse in B-scan image is not visible at all. Also the combination of SE and CFE in same model does not cause any significant numerical errors (**Fig. 26**b).

CONCLUSIONS

1. Numerical errors in FE models are inevitable and caused by the size of discretization step of the mesh of FE model and depends on the frequency spectra of the simulated wave. Conventional FE models assembled of consistent or lumped mass matrices generate similarly valued but opposite sign numerical errors. Methods for reducing these errors are basically based on the applications of higher-order FE, combined mass matrix or synthesized elements. Unfortunately, in all these cases, the mass matrices in FE model are non-diagonal and do not allow to exploit the advantages of explicit integration schemes.
2. An algorithm was created for the construction of 1D and 2D synthesized finite element with a diagonal mass matrix applying a mode synthesis procedure. Mode corrections are performed to obtain the synthesized elements, while the correction coefficients are the parameters of target function, while the target function evaluates the errors of mode frequencies of the sample model consisting of synthesizing elements. It is demonstrated that a larger number of degree of freedom in the synthesized element leads to better convergence properties.
3. An investigation of the convergence of the models in a one-dimensional structure has revealed that the errors for the first ~60% mode frequencies in the models composed of 10 nodes, the synthesized elements are not

significant ($< 10^{-6}$). A branched non-homogenous structure can be assembled from the synthesized elements, where a combination of these elements with conventional elements allows to implement a non-reflection boundary condition.

4. The analysis of a 2D model convergence has shown that the necessary demand for computational resources in element synthesis can be reduced by applying the properties of symmetric modes. As a result, 5×5 nodes acoustic and 4×4 nodes elastic squared synthesized elements have been constructed. The errors of first 25% (in acoustic model) and 6.2% (in elastic model) of mode frequencies in the model consisting of synthesized elements are insignificant. By performing a simulation in 2D elastic models, small errors (~2% of size of simulated impulse) occur; however, the spatial and time locations of these errors are easily predictable and they can be eliminated in impulse analysis after simulation.
5. The synthesized elements have been verified in numerical experiments. The fluid flow model was created for transient analysis of a one-dimensional structure in pipelines. In the cases of 2D models, ultrasonic measurements have been simulated. The investigation has shown that models comprised of 10 nodes 1D, 2D acoustic (5×5 nodes) and 2D elastic (4×4) synthesized elements allowed to use coarser meshes (approximately for 1D ~4.7 times; 2D acoustic ~2.5 times; 2D elastic ~2 times) with the same model accuracy. The performance tests have shown that greater bandwidth of stiffness matrix in models of synthesized elements caused by higher order elements is not significant, and in all cases the computer memory and computational resources necessary for wave simulation are saved.

REFERENCES

Barauskas, R. (2005). On highly convergent 2D acoustic and elastic wave propagation models. *Communications in Numerical Methods in Engineering*, *22*(3), 225–233. http://doi.org/10.1002/cnm.810

Barauskas, R., & Barauskiene, R. (2004). Highly convergent dynamic models obtained by modal synthesis with application to short wave pulse propagation. *International Journal for Numerical Methods in Engineering*, *61*(14), 2536–2554. http://doi.org/10.1002/nme.1169

He, Z. C., Li, E., Liu, G. R., Li, G. Y., & Cheng, A. G. (2016). A mass-redistributed finite element method (MR-FEM) for acoustic problems using triangular mesh. *Journal of Computational Physics*, *323*, 149–170. http://doi.org/10.1016/j.jcp.2016.07.025

Ihlenburg, F., & Babuska, I. (1995). Dispersion Analysis and Error Estimation of Galerkin Finite Element Methods for the Helmholtz Equation. *International Journal for Numerical Methods in Engineering*,

38(December 1994), 3745–3774. http://doi.org/10.1137/040605278
Yue, B., & Guddati, M. N. (2005). Dispersion-reducing finite elements for transient acoustics. *Journal of the Acoustical Society of America*, *118*(4), 2132–2141. http://doi.org/10.1121/1.2011149
Jie, C., Xin, G., & Gangtie, Z. (2015). A simultaneous iterative procedure for the Kron's component modal synthesis approach. *Proceedings of the 2011 American Control Conference*, (March), 990–1013. http://doi.org/10.1002/nme
Khajavi, R. (2014). General templates for n-noded bar elements based on reduced representations and numerical dispersion reduction by optimized finite elements. *Applied Mathematics and Computation*, *233*, 445–462. http://doi.org/10.1016/j.amc.2014.02.022
Li, E., He, Z. C., Zhang, Z., Liu, G. R., & Li, Q. (2016). Stability analysis of generalized mass formulation in dynamic heat transfer. *Numerical Heat Transfer, Part B: Fundamentals*, *69*(4), 287–311. http://doi.org/10.1080/10407790.2015.1104215
Mirbagheri, Y., Nahvi, H., Parvizian, J., & Düster, A. (2015). Reducing spurious oscillations in discontinuous wave propagation simulation using high-order finite elements. *Computers & Mathematics with Applications*, *70*(7), 1640–1658. http://doi.org/10.1016/j.camwa.2015.06.022
Moser, F., Jacobs, L. J., & Qu, J. (1999). Modeling elastic wave propagation in waveguides with the finite element method. *NDT & E International*, *32*(4), 225–234. http://doi.org/10.1016/S0963-8695(98)00045-0
Noh, G., & Bathe, K. J. (2013). An explicit time integration scheme for the analysis of wave propagations. *Computers and Structures*, *129*, 178–193. http://doi.org/10.1016/j.compstruc.2013.06.007
Żak, a., & Krawczuk, M. (2011). Certain numerical issues of wave propagation modelling in rods by the Spectral Finite Element Method. *Finite Elements in Analysis and Design*, *47*(9), 1036–1046. http://doi.org/10.1016/j.finel.2011.03.019
Zuo, Z., Li, S., Zhai, C., & Xie, L. (2014). Optimal Lumped Mass Matrices by Minimization of Modal Errors for Beam Elements. *Journal of Vibration and Acoustics*, *136*(2), 21015. Retrieved from http://dx.doi.org/10.1115/1.4026247

A LIST OF PUBLICATIONS ON THE TOPIC OF DISSERTATION

Indexed in the Web of Science with Impact Factor

1. Kriščiūnas, A., & Barauskas, R. (2016). Highly Convergent Finite Elements with Diagonal Mass Matrix for Short Wave Pulse Propagation Simulation. Information Technology And Control, 45(3), 308–320.

2. Barauskas, R., Kriščiūnas, A., & Blažauskas, T. (2016). A finite element model in a form of structural dynamic equation for the transient analysis of pressure in pipelines. Journal of Vibroengineering, 18(2), 1209–1226.

Indexed in the Web of Science without Impact Factor

3. Prikšaitis, J., Mažeika, L., Barauskas, R., Žukauskas, E., & Kriščiūnas, A. (2015). Influence of the Numerical Dispersion Effects in the Modelling of Ultrasonic Measurements. *Physics Procedia*, *70*, 532-536.
4. Krisciunas, A., & Barauskas, R. (2013, October). Minimization of Numerical Dispersion Errors in Finite Element Models of Non-homogeneous Waveguides. In *ICIST* (pp. 357-364).

Publications in other international databases (Articles in periodicals, collections of articles and conference proceedings)

1. Kriščiūnas, A., Barauskas, R., Mažeika, L., & Fyleris, T. (2016, October). Minimization of Numerical Dispersion Errors in 2D Finite Element Models of Short Acoustic Wave Propagation. In *International Conference on Information and Software Technologies* (pp. 745-752). Springer International Publishing.

Articles in other peer-reviewed research publications

1. Patasius, M., Krisciunas, A., Rapalis, A., Barauskas, R., Janusauskas, A., Calneryte, D., & Neciunas, A. (2016). Exploration of modelling of blood flow through the arterial tree using phase error reducing finite element model. *Biomedical Engineering 2016*, *20*(1).

REZIUMĖ

Bangų sklidimą tampriosiose ir akustinėse terpėse tenka modeliuoti sprendžiant daugybę inžinerinių uždavinių, tarp kurių mechaninių konstrukcijų reakcijos į dinaminį žadinimą apskaičiavimas, ultragarso matavimų schemų ir rezultatų analizės algoritmų projektavimas ir testavimas, pavojingų slėgio impulsų sklidimo vamzdynuose prognozavimas ir trūkio vietos aptikimas pagal sklindančios bangos požymius, seisminių bangų sklidimo Žemės gelmėse ir paviršiuje apskaičiavimas ir kt.

Iš pirmo žvilgsnio minėtus bangų sklidimo procesus modeliuoti nesudėtinga. Dažnai jie išreiškiami tiesinėmis kontinuumo mechanikos lygtimis, kurios gali būti skaitiškai išspręstos diskretizuojant erdvėje bei laiko intervale ir taikant baigtinių skirtumų metodą (BSM), baigtinių elementų metodu (BEM) paremtas arba kombinuotąsias skaitines schemas. BEM formuluotės tampriosioms bangoms modeliuoti žinomos jau nuo 1960–1970 metų. Jų matematiniai principai išliko iš esmės nepakitę iki šiol. Skaitiniai bangų sklidimo algoritmai pritaikyti tiek universaliose BEM programinės įrangos sistemose (*ANSYS*, *MSC*, *ABACUS*,

COMSOL ir kt.), tiek specializuotose bangų sklidimui modeliuoti skirtose programose (*WAVE2000*, *WAVE3000*).

Skaitiniai bangų sklidimo modeliai iš principo yra matematiškai ir programiškai nesudėtingi, tačiau turi jiems būdingą silpnąją vietą. Tai sunkiai atpažįstamos skaičiavimo paklaidos, kurios susidaro panaudojus bent kiek retesnį erdvės tinklelį. Gerai žinoma, kad objekto, kuriame modeliuojamas bangos sklidimas, erdvės tinklelis turėtų būti ne retesnis nei 17–20 BE modeliuojamos bangos ilgyje. Skaičiuotojai praktikai iš patirties žino, kad tai labai nekonservatyvus (nors dažnai literatūroje minimas) įvertis, ir pasirenka dar smulkesnį – maždaug 30 BE bangos ilgyje – tinklelį. Pernelyg reto tinklelio nulemtos paklaidos pavojingos tuo, kad jas labai sunku atpažinti analizuojant gautus skaitinius sprendinius. Dažnai paklaidų dedamosios vizualiai nesiskiria nuo įprastinių konstrukcijoje sklindančių bangų. Jos pasireiškia kaip aukštesniojo dažnio bangos, sklindančios pagrindinės bangos priekyje arba gale. Tokio pobūdžio bangos gali būti ir tikrovėje generuojamos dėl terpės geometrinių nehomogeniškumų, kuriuos savo kelyje sutinka pagrindinė banga. Taip pat jos gali kilti dėl tuo pat metu sužadintų aukštesniojo dažnio paviršinių bangų atspindžių ir pan. Tačiau tokio pobūdžio modelyje stebimų bangų priežastimi gali būti ir skaitinės paklaidos. Kartais jos populiariai vadinamos skaitiniu triukšmu arba difrakcija nuo tinklelio mazgų. Tačiau esmė visada ta pati – nepakankamas tinklelio smulkumas. Kokį jį reikėtų parinkti, iš anksto numatyti nelengva. Sužadinant bet kurią bangą, dalyvauja ne tik pagrindinė, bet ir visos harmoninės jos komponentės. Skaitines paklaidas gali sugeneruoti bet kuri iš jų. Vienintelė universali priemonė skaitinėms paklaidoms atpažinti yra BE modelio pateikiamo sprendinio konvergavimo analizė sulyginant kelias to paties proceso realizacijas, gautas su skirtingo smulkumo modelio tinkleliais.

Labai tankaus tinklelio poreikis kelia problemų, kai tiriamos srities matmenys yra gerokai didesni už joje sklindančių bangų ilgį. Iš čia kyla trumposios bangos sąvoka, kuri daugiau susijusi su bangos sklidimo modeliais diskrečiaisiais tinkleliais pateiktose srityse nei su absoliučiaisiais geometriniais dydžiais. Banga laikoma trumpąja tada, kai jos ilgis daug kartų mažesnis už viso modelio būdinguosius geometrinius matmenis. Pavyzdžiui, reikia išspręsti plokščiųjų bangų sklidimo plieninėje 10×10 cm dydžio plokštelėje uždavinį, kai žadinamų skersinių bangų dažnis yra 10 Mhz (ultragarso bangos). Esant ~3000 m/s bangos greičiui ir atitinkamai 0,03 mm bangos ilgiui, išilgai plokštelės tilptų ~300 bangos ilgių, o tinklelio žingsnį tektų parinkti ~0,1 mm. Taip būtų tenkinama 20–30 tinklelio žingsnių bangos ilgyje sąlyga. Vadinasi, modelio mazgų skaičius netgi tokio palyginti nesudėtingo uždavinio atveju turėtų būti ~10000×10000. Skaitiškai reikėtų spręsti $\sim 10^8$ lygčių sistemą, kai banga akustinė, ir $\sim 20^8$ lygčių sistemą, kai banga tamprioji.

Taigi viena svarbiausių problemų, kylančių skaitiškai modeliuojant trumpųjų bangų sklidimą, yra itin didelis skaičiavimo išteklių poreikis. Sukūrus

aukštesniosios eilės baigtinius elementus, užtikrinančius sprendinio konvergavimą esant 2–3 kartus retesniam tinkleliui, sprendžiamo uždavinio matmenys gali sumažėti 10–30 kartų. Šiame darbe siekiama sukurti naujus, greičiau konverguojančius baigtinius elementus akustinių ir tampriųjų bangų skaitiniams modeliams.

Tyrimo objektas – aukštesniosios tikslumo eilės baigtiniai elementai, skirti tampriųjų ir akustinių trumpųjų bangų sklidimo baigtinių elementų modelių paklaidoms sumažinti.

Tyrimo tikslas – sukurti algoritmus aukštosios tikslumo eilės tampriojo ir akustinio kontinuumo baigtinių elementų sintezei, kurie leistų gerokai sumažinti skaičiavimo išteklių poreikį sklindančios bangos modeliavimui inžineriškai priimtinu tikslumu, ir ištirti gautų elementų savybes taikant juos homogeninėse ir nehomogeninėse struktūrose.

Tyrimo uždaviniai

Tyrimo tikslui pasiekti iškelti šie uždaviniai:

1. Išanalizuoti BE modeliuose atsirandančių fazinio greičio paklaidų kilmę ir žinomus šių paklaidų minimizavimo būdus.
2. Taikant modų sintezės metodą, pagal optimaliai pakoreguotas modas sintezuoti vienmačius (1D) ir dvimačius (2D) mažiausios fazinės paklaidos baigtinius elementus, kurių masių matrica yra įstrižainininė.
3. Ištirti sintezuotaisiais elementais paremtų bangos sklidimo modelių konvergavimą nehomogeniniuose ir šakotuose 1D tinkluose.
4. Ištirti sintezuotaisiais elementais paremtų akustinių ir tampriųjų bangų modelių konvergavimą nehomogeniniuose sudėtingos geometrinės formos 2D tinkluose.
5. Verifikuoti sukurtus baigtinius elementus ir ištirti iš jų sukurtų modelių privalumus ir našumą, palyginant su iš įprastinių baigtinių elementų sudarytais modeliais.

Darbo mokslinis naujumas

Darbe sukurtas naujas algoritmas, leidžiantis optimaliai koreguotų modų sintezės būdu apskaičiuoti baigtinius elementus, iš kurių surinkti modeliai turi daug platesnį artimų tiksliems tikrinių dažnių ruožą nei modeliai, gauti iš iki šiol žinomų baigtinių elementų. Nors iš principo koreguotų modų sintezės būdas aukštosios tikslumo eilės baigtiniams elementams gauti buvo pritaikytas jau anksčiau, šiame darbe gautų elementų masių matricos yra įstrižainininės ir tinkamos naudoti išreikštinio dinaminio modeliavimo (angl. *explicit dynamics*) skaitinėse schemose.

Darbo praktinė vertė

Kitaip nei įprastiniai modų sintezės būdu gauti elementai, šiame darbe sukurti elementai gali būti tiesiogiai panaudoti išreikštinio dinaminio modeliavimo programinėje įrangoje. Taikomieji skaičiavimai buvo atlikti tiriant realius bangų sklidimo principu veikiančius ultragarso matavimų modelius.

Darbo rezultatų aprobavimas

Disertacijos tema paskelbti 6 moksliniai straipsniai, 2 iš jų – Mokslinės informacijos instituto (ISI) pagrindinio sąrašo leidiniuose, turinčiuose citavimo indeksą. Disertacijos tema atliktų tyrimų rezultatai buvo pristatyti 4 mokslinėse konferencijose Lietuvoje ir užsienyje.

Bendrosios išvados

1. Skaitiškai modeliuojant bangą BE modeliuose visada atsiranda skaitinių paklaidų, kurios priklauso nuo tinklelio diskretizavimo žingsnio ir simuliuojamo impulso dažnių spektro. Tradiciniai baigtinių elementų modeliai, gauti panaudojant sutelktąsias arba konsistentines masių matricas, generuoja panašaus dydžio, tačiau priešingų ženklų paklaidas. Iki šiol žinomi būdai sumažinti šias paklaidas yra paremti aukštesniosios eilės baigtiniais elementais arba kombinuotosiomis bei sintezuotosiomis masių matricomis. Deja, tokios masių matricos yra neįstrižainės, todėl neleidžia visiškai panaudoti išreikštinių skaitinio integravimo schemų privalumų.

2. Taikant modų sintezės metodą sukurtas algoritmas, skirtas 1D ir 2D sintezuotiesiems baigtiniams elementams su įstrižainėmis masių matricomis sudaryti. Sintezuotieji elementai sudaromi atliekant elemento virpesių modų korekcijas, kur modų korekcijos koeficientai yra tikslo funkcijos minimizavimo parametrai, o pati tikslo funkcija apibrėžia modelio, surinkto iš sintezuotųjų elementų, pirmųjų tikrinių dažnių paklaidas. Pademonstruota, kad didesnis sintezuojamo elemento laisvės laipsnių skaičius lemia geresnes sintezuotojo elemento konvergavimo savybes.

3. Ištyrus modelių konvergavimą 1D struktūrose pademonstruota, kad, BE modelį surenkant iš sintezuotųjų 10 mazgų elementų, pirmųjų ~60 % modelio tikrinių dažnių paklaidos būna labai mažos ($<10^{-6}$). Iš šių elementų galima sudaryti šakotą nehomogeninę struktūrą ir modelį surenkant kartu su tradiciniais elementais įvertinti bangos neatspindėjimo sąlygą.

4. Ištyrus modelių konvergavimą 2D struktūrose, nustatyta, kad skaičiavimo išteklių poreikis sintezės procesui gali būti sumažintas pasinaudojant simetrinių konstrukcijų modų savybėmis, ir atsižvelgiant į turimus skaičiavimo išteklius sudarytas 5×5 mazgų akustinis ir 4×4 mazgų kvadrato formos tamprusis elementas. Modelių, surinktų iš tokių elementų, pirmųjų 25 % (akustiniuose modeliuose) ir 6,2 % (tampriuosiuose modeliuose) tikrinių dažnių paklaidos

išlieka labai mažos. Nors atliekant impulso modeliavimą 2D tampriuosiuose modeliuose, surinktuose iš sintezuotųjų elementų, dėl atliktų konstrukcijos modų korekcijų papildomai atsiranda nedidelės (~2 % modeliuojamo impulso amplitudės) paklaidos, jų vieta yra nuspėjama ir šios paklaidos gali būti nesunkiai pašalinamos atliekant signalo analizę.

5. Sintezuotieji elementai verifikuoti atliekant skaitinius tyrimus. Sukurtas 1D spūdaus skysčio tėkmės baigtinių elementų modelis, skirtas pereinamiesiems virpesiams vamzdyne apskaičiuoti. 2D konstrukcijose buvo simuliuojami testiniai realių ultragarso matavimų atvejai. Atliekant skaitinius tyrimus nustatyta, kad sudaryti 10 mazgų 1D, 2D akustiniai (5×5 mazgų) ir 2D tamprieji (4×4 mazgų) sintezuotieji elementai leido panaudoti gerokai retesnius tinklelius (1D – 4,7 karto; 2D akustinis – 2,5 karto; 2D tamprusis – 2 kartus), išlaikant tokį patį sprendinio tikslumą. Tinklelio retumas verifikuojamas pagal konkretaus simuliuojamo impulso dažnių spektrą ir BE modelio tikrinių dažnių paklaidas atliekant pasirinkto impulso modeliavimą skirtingo retumo tinklelio modeliuose. Atliekant našumo testus nustatyta, kad panaudojus aukštesniosios eilės sintezuotuosius elementus gautas didesnis standumo matricos juostos plotis didesnės reikšmės neturi ir visais atvejais yra sutaupoma kompiuterio atmintis, reikalinga BE modeliui saugoti, ir sumažinamos skaičiavimo, atliekamo modeliuojant bangą, apimtys.

UDK 519.65:531 (043.3)

SL344. 2017-06-22, 2,5 leidyb. apsk. l. Tiražas 50 egz.
Išleido Kauno technologijos universitetas, K. Donelaičio g. 73, 44249 Kaunas
Spausdino leidyklos „Technologija“ spaustuvė, Studentų g. 54, 51424 Kaunas